Acta Crystallographica Section D
**Biological Crystallography**
ISSN 0907-4449

# 1.2 Å resolution crystal structure of *Escherichia coli* WrbA holoprotein

**Iryna Kishko,[a,b] Jannette Carey,[c]* David Reha,[a,b] Jiri Brynda,[d] Renee Winkler,[c] Balasubramanian Harish,[c] Richard Guerra,[c] Olga Ettrichova,[a,b] Zdenek Kukacka,[e,f] Olena Sheryemyetyeva,[a,b] Petr Novak,[e,f] Michal Kuty,[a,b] Ivana Kuta Smatanova,[a,b] Rüdiger Ettrich[a,b]* and Mikalai Lapkouski[a,b]***

[a]Institute of Nanobiology and Structural Biology, Global Change Research Center, Academy of Sciences of the Czech Republic, Zamek 136, 37333 Nove Hrady, Czech Republic, [b]Faculty of Sciences, University of South Bohemia, Branisovska 31, 370 05 Ceske Budejovice, Czech Republic, [c]Department of Chemistry, Princeton University, Princeton, NJ 08544-1009, USA, [d]Institute of Molecular Genetics and Institute of Organic Chemistry and Biochemistry, Academy of Sciences of the Czech Republic, Flemingovo nam. 2, 16610 Prague 6, Czech Republic, [e]Institute of Microbiology, Academy of Sciences of the Czech Republic, Videnska 1083, 14220 Prague 4, Czech Republic, and [f]Department of Biochemistry, Faculty of Science, Charles University Prague, Hlavova 8, 12843 Prague 2, Czech Republic

Correspondence e-mail: jcarey@princeton.edu, ettrich@nh.cas.cz, lapkouski@nh.cas.cz



Received 15 January 2013
Accepted 20 June 2013

**PDB Reference:** WrbA, 3zho

The *Escherichia coli* protein WrbA, an FMN-dependent NAD(P)H:quinone oxidoreductase, was crystallized under new conditions in the presence of FAD or the native cofactor FMN. Slow-growing deep yellow crystals formed with FAD display the tetragonal bipyramidal shape typical for WrbA and diffract to 1.2 Å resolution, the highest yet reported. Faster-growing deep yellow crystals formed with FMN display an atypical shape, but diffract to only ∼1.6 Å resolution and are not analysed further here. The 1.2 Å resolution structure detailed here revealed only FMN in the active site and no electron density that can accommodate the missing parts of FAD. The very high resolution supports the modelling of the FMN isoalloxazine with a small but distinct propeller twist, apparently the first experimental observation of this predicted conformation, which appears to be enforced by the protein through a network of hydrogen bonds. Comparison of the electron density of the twisted isoalloxazine ring with the results of QM/MM simulations is compatible with the oxidized redox state. The very high resolution also supports the unique refinement of Met10 as the sulfoxide, confirmed by mass spectrometry. Bond lengths, intramolecular distances, and the pattern of hydrogen-bond donors and acceptors suggest the cofactor may interact with Met10. Slow incorporation of FMN, which is present as a trace contaminant in stocks of FAD, into growing crystals may be responsible for the near-atomic resolution, but a direct effect of the conformation of FMN and/or Met10 sulfoxide cannot be ruled out.

## 1. Introduction

The 21 kDa gene product WrbA from *Escherichia coli* (Yang *et al.*, 1993) was identified as the founding member of a family of flavodoxin-like proteins conserved from bacteria to higher plants that are implicated in cellular responses to altered redox conditions and other types of stress (Grandori & Carey, 1994). The exact physiological role of WrbAs is still unknown, but available evidence is consistent with a role in oxidative stress defence and/or cell signalling. WrbAs are related by remote homology to flavodoxins, but have significant distinctions. Unlike simple flavodoxins, *E. coli* WrbA is multimeric (Grandori *et al.*, 1998). Crystal structures of WrbAs (Gorman & Shapiro, 2005; Andrade *et al.*, 2007; Carey *et al.*, 2007) confirm that monomers adopt the $\alpha/\beta$ twisted open-sheet fold typical of flavodoxins, but they present no separate domains that support the observed tetrameric assembly (Wolfova *et al.*, 2009). *E. coli* WrbA specifically binds one FMN per monomer but with much lower affinity than typical flavodoxins [$K_d$ in the range $10^{-5}$–$10^{-6}$ *M* (Grandori *et al.*, 1998) *versus* $10^{-7}$–$10^{-10}$ *M* (Mayhew & Tollin, 1991)]. *E. coli* and *Archeoglobus fulgidus* WrbAs display FMN-dependent NAD(P)H:quinone

oxidoreductase (Nqo) activity (Patridge & Ferry, 2006). Like other Nqos, including the dimeric FAD-dependent mammalian diaphorase (Li *et al.*, 1995), *E. coli* WrbA transfers pairs of electrons from NADH to various quinone electron acceptors with no stable FMN semiquinone detected during the electron-transfer reaction (Nöll *et al.*, 2006), whereas the flavodoxins transfer single electrons to protein acceptors *via* a stable FMN semiquinone (Mayhew & Tollin, 1991). WrbAs thus appear to bridge the simple monomeric FMN-dependent bacterial flavodoxins and the multimeric FAD-dependent mammalian Nqos (Carey *et al.*, 2007).

Early assays of the WrbA redox reaction (Fig. 1*a*) suggested that the Nqo activity of *E. coli* WrbA is supported by FAD, but with approximately tenfold more FAD required to yield an activity equivalent to that with FMN. Early analyses of FAD stocks by thin-layer chromatography (data not shown) seemed to rule out the possibility that ∼10% FMN could be present to account for this activity. These facts motivated the attempted crystallization of *E. coli* WrbA with FAD as a cofactor, although only FMN was observed in the resulting crystals in several independent trials. These crystals diffracted to near-atomic (1.2 Å) resolution, allowing new structural inferences to be made about the WrbA–FMN complex, as reported here. Subsequent analyses of the WrbA redox activity with FAD, informed by recent studies of its kinetic mechanism (Kishko *et al.*, 2012) with optimal conditions and concentrations of NADH and quinone substrates, combined with quantitative analysis of FMN contamination in FAD stocks by HPLC, revealed that traces of FMN in the kinetic assays can indeed account for the early results that had suggested that FAD could support WrbA redox activity.

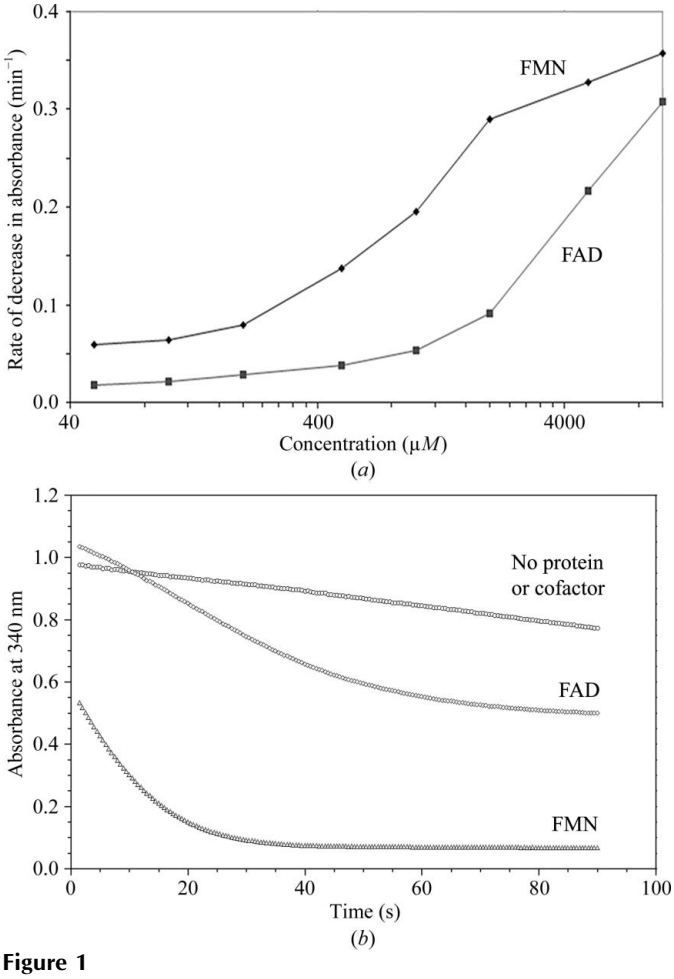


**Figure 1**
Apparent redox activity of WrbA with FAD. (*a*) Flavin concentration dependence. The initial rate of decrease in the absorbance at 340 nm with time as in (*b*) is plotted as a function of the log of flavin concentration. Diamonds, FMN; squares, FAD. (*b*) Initial velocity. The absorbance at 340 nm is plotted *versus* time with 1 μ*M* FMN (triangles), with 100 μ*M* FAD (diamonds) or with no protein or cofactor (circles). The first ∼20 s (FMN) or ∼40 s (FAD) represents the initial rate of decrease as in (*a*). Although both plots suggest that FAD supports WrbA redox activity, quantitation of flavin stocks by HPLC (not shown) indicates that the apparent activity can be accounted for by FMN contamination of FAD stocks.

## 2. Materials and methods

### 2.1. Protein expression, purification and holoprotein reconstitution

Similarly as in the previously described procedure (Grandori *et al.*, 1998), WrbA was expressed in *E. coli* BL21(λDE3) cells and purified in 20 m*M* sodium phosphate, 1 m*M* EDTA but using DEAE-Sepharose (HiPrep, Sigma) before the Affi-Gel Blue (Bio-Rad) affinity column. The initiator methionine is cleaved from the mature *E. coli* WrbA (Grandori *et al.*, 1998) and the residue numbering used here follows that of Grandori *et al.* (1998) starting with Ala1. The concentration of the purified apoprotein after dialysis in 20 m*M* Tris–HCl pH 7.5 was determined by UV absorption spectroscopy using the monomer extinction coefficient $\varepsilon_{280}$ = 22 831 $M^{-1}$ cm$^{-1}$. WrbA holoprotein with FAD or FMN was prepared for crystallization by incubation of 0.25 m*M* apoprotein (monomer) with 0.35 m*M* FAD or FMN (Sigma), as described previously for cocrystallization with FMN (Wolfova *et al.*, 2009). Under these conditions at equilibrium >90% of the apoprotein is present in the form of tetramers and the FMN occupancy is ∼98% as calculated from the data presented by Grandori *et al.* (1998). Using the estimated tenfold weaker binding of FAD than FMN based on earlier redox assays, the FAD occupancy was predicted to be 86%.

### 2.2. Enzyme activity

The redox activity of WrbA with FAD or FMN as cofactor was assayed by monitoring the oxidation of NADH at 340 nm. Initial assays such as those shown in Fig. 1(*a*) used 20 n*M* WrbA, 100 μ*M* NADH and 250 μ*M* benzoquinone in 20 m*M* sodium phosphate pH 6.5, 1 m*M* EDTA. Later assays such as those shown in Fig. 1(*b*) used 20 n*M* WrbA and the indicated concentration of cofactor, 250 μ*M* NADH and 500 μ*M* benzoquinone in 20 m*M* sodium phosphate pH 7.2 (Kishko *et al.*, 2012). In both cases reactions were started by the addition of WrbA holoprotein formed by pre-incubation of apo WrbA with cofactor on ice for ∼1 h. Reactions were carried out in a 1 cm path-length cuvette at room temperature with a total volume of 1 ml and were monitored for at least 60 s.

**Table 1**
Data-collection and refinement statistics for WrbA–(FAD).

Values in parentheses are for the highest resolution shell.

| | |
|---|---|
| Data-collection statistics | |
| Radiation source | MX-14.2, BESSY II |
| Detector | MAR Mosaic CCD 225 mm |
| Wavelength (Å) | 0.9171 |
| No. of images | 200 |
| Rotation range per image (°) | 0.5 |
| Resolution range (Å) | 22.71–1.20 (1.23–1.20) |
| Space group | $P4_12_12$ |
| Unit-cell parameters (Å, °) | $a = b = 61.15$, $c = 169.6$, $\alpha = \beta = \gamma = 90$ |
| Measured reflections | 732496 (27490) |
| Unique reflections | 97715 (5478) |
| Multiplicity | 7.6 (5.0) |
| Wilson $B$ (Å$^2$) | 10.2 |
| Mosaicity (°) | 0.2 |
| Completeness (%) | 96.6 (75.1) |
| $R_{\rm merge}$† (%) | 6.4 (68.0) |
| $\langle I/\sigma(I)\rangle$ | 14.3 (2.2) |
| Refinement statistics | |
| Resolution range (Å) | 21.46–1.20 (1.23–1.20) |
| No. of reflections (working/test set) | 92773 (5236)/4864 (244) |
| $R_{\rm work}/R_{\rm free}$‡ (%) | 14.73 (27.1)/17.04 (27.5) |
| No. of atoms | |
| Protein | 2807 |
| FMN | 93 |
| Solvent | 318 |
| $\langle B\rangle$ (Å$^2$) | |
| Protein | 15.09 |
| FMN | 11.76 |
| Solvent | 29.53 |
| R.m.s. deviations | |
| Bond lengths (Å) | 0.008 |
| Bond angles (°) | 1.37 |
| Ramachandran plot (%) | |
| Residues in most favoured regions | 100 |
| PDB code | 3zho |

† $R_{\rm merge} = \sum_{hkl}\sum_i |I_i(hkl) - \langle I(hkl)\rangle| / \sum_{hkl}\sum_i I_i(hkl)$, where $I_i(hkl)$ is the intensity of the $i$th measurement of reflection $hkl$ and $\langle I(hkl)\rangle$ is the average intensity of the reflection. ‡ $R = \sum_{hkl} \big||F_{\rm obs}| - |F_{\rm calc}|\big| / \sum_{hkl} |F_{\rm obs}|$, where $F_{\rm obs}$ represents the observed structure factors and $F_{\rm calc}$ the calculated structure factors based on the model. $R_{\rm work}$ was calculated based on the working set of reflections used in the refinement and $R_{\rm free}$ was calculated based on the test set of reflections excluded from refinement.

### 2.3. Thin-layer chromatography

WrbA at 0.25 m*M* (monomer) with 0.35 m*M* FAD, and control samples of FMN and FAD without protein, were incubated for various times at ∼297 K in 10 m*M* sodium phosphate buffer pH 7.2, 1 m*M* EDTA or in the crystallization conditions reported here. Protein-containing samples were extracted with five volumes of methanol and centrifuged for 1 min at 14 000 rev min$^{-1}$. The supernatant was dried in air at room temperature and dissolved in one volume of water. Samples were spotted on silica-gel plates (SIL G-25, thickness 0.25 mm) and developed in the dark with a mobile phase of butanol:acetic acid:water (12:3:5). Fluorescence was detected under UV light.

### 2.4. HPLC

Flavin stocks prepared in water were diluted into 50 m*M* acetate buffer pH 4, 20% acetonitrile and loaded onto an MC18 Chromegabond reverse-phase column (ES Industries; 25 cm × 4.6 mm, 5 µm particle size, 100 Å pores) on a Waters 600S HPLC using a 20 µl loop. The column was developed at a flow rate of 1.5 ml min$^{-1}$ with a 21 min linear gradient from 10 to 50% acetonitrile in 50 m*M* acetate buffer pH 4, 1% triethylamine. The elution of flavins was detected by monitoring absorbance at 335 nm.

### 2.5. Crystallization

Crystallizations were initially performed in Cryschem 24-well plates (Hampton Research, Aliso Viejo, USA) using the sitting-drop vapour-diffusion technique and subsequently with the hanging-drop method (Ducruix & Giegé, 1999) with similar results. Drops consisting of 1–2 µl protein solution and 1 µl reservoir solution were equilibrated against 700 µl reservoir solution consisting of 28% PEG 3350, 0.05 *M* bis-tris–HCl pH 6.5, conditions which differ slightly from those reported previously for WrbA-FMN (Wolfova *et al.*, 2009). All crystallizations were carried out at 288 K. Under these conditions using FAD, deep yellow tetragonal bipyramidal crystals typical of those obtained for WrbA-FMN under other conditions (Wolfova *et al.*, 2009) grew within several weeks. Using FMN in the present conditions, rod-shaped crystals with the same deep yellow colour appeared overnight and grew to their final dimensions in ∼4 d. In previously reported conditions tetragonal bipyramidal crystals of WrbA-FMN grew within one week (Wolfova *et al.*, 2009).

### 2.6. X-ray data collection, structure solution and refinement

Four-week-old crystals of WrbA grown with FAD and freshly grown (∼5 d old) crystals of WrbA grown with FMN were used for the diffraction experiments reported here. Diffraction data were collected on beamline BL14.2 operated by the Joint Berlin MX-Laboratory at the BESSY II electron-storage ring (Berlin-Adlershof, Germany; Mueller *et al.*, 2012) using a MAR CCD 225 mm detector. Crystals were flash-cooled in a nitrogen stream at 100 K without additional cryoprotection. For the crystals grown with FAD, a total of 200 diffraction images were collected using a 0.5° oscillation angle. The measured data were integrated using *MOSFLM* (Leslie, 2006) and scaled using *SCALA* (Evans, 2006). Data-collection statistics are presented in Table 1. The structure was solved by molecular replacement using the program *MOLREP* (Vagin & Teplyakov, 2010). Refinement was carried out with *REFMAC* (Murshudov *et al.*, 2011) and included restrained individual coordinate refinement and anisotropic refinement of atomic displacement parameters for all atoms including 318 water molecules. Manual building and model correction was performed in *Coot* (Emsley & Cowtan, 2004). Comprehensive validation of the model with diffraction data was performed with the validation tool in *PHENIX* (Adams *et al.*, 2010), which includes *MolProbity* analysis (Chen *et al.*, 2010) of the protein geometry. The final model has an $R$ factor of 14.73% and an $R_{\rm free}$ of 17.04%, with 100% of the residues in Ramachandran favoured regions. Refinement statistics are given in Table 1. Analyses of surface areas and interactions were made using the *PISA* server (Krissinel & Henrick, 2007). Figures were produced with *PyMOL* (http://www.pymol.org; Schrö-

dinger). Structure and experimental data have been deposited in the PDB as entry 3zho.

### 2.7. Refinement with H atoms

To preserve the observed propeller twist, H atoms were added to FMN in the conformation observed in the 1.2 Å resolution structure reported here. Subsequent manipulations were performed using programs from the *PHENIX* package (Adams *et al.*, 2010). Explicit H atoms were added to the protein using *ReadySet* in *PHENIX*. H atoms and restraints for FMN were generated in *phenix.elbow*. Hydrogen positions were corrected in *phenix.reel*. Planar restraints of the isoalloxazine plane were loosened and refinement of the atomic coordinates and anisotropic *B* factors for all atoms (excluding H atoms) was performed in *phenix.refine*. Atomic contacts were analyzed by *phenix.probe* and displayed in *Coot*. Fig. 2(*d*) was prepared by rendering a scene in *Coot* with *Raster3D* (Merritt & Bacon, 1997) and was prepared using *CCP4mg* (McNicholas *et al.*, 2011).

### 2.8. Mass spectrometry

Apo WrbA was dissolved in 20 m*M* HEPES buffer pH 7.2 to 0.2 m*M* (monomer) with FMN added to a final concentration of 0.7 m*M*. Aliquots containing 10 µg WrbA were collected by isolation of WrbA using MicroTrap columns (Michrom Bioresources, California, USA). Samples were loaded onto the columns in 1% acetic acid, washed with 1% acetic acid/10% acetonitrile and eluted with 1% acetic acid/80% acetonitrile. Purified proteins were diluted 20-fold in 0.1% formic acid/50% methanol. Mass spectra were acquired in positive-ion mode on an APEX-Ultra FTMS instrument equipped with a 9.4 T superconducting magnet and a Dual II electrospray-ionization ion source (Bruker Daltonics, Billerica, Massachusetts, USA). The cell was opened for 1.6 ms and the accumulation time was set to 0.4 s for MS experiments and 3.0 s for MS/MS experiments, where one experiment consists of the average of eight spectra for MS and 64 spectra for MS/MS. The most intense charge states of the parent ions were fragmented by collision-induced dissociation. The isolation window was set to 3 Da and the collision energy to 7 V. The acquisition data-set size was 512 000 points with the mass range starting at $m/z$ 300 Da, resulting in a resolution of 200 000 at $m/z$ 400 Da. The instrument was externally calibrated using clusters of arginine, resulting in a mass accuracy of <2 p.p.m. The acquired spectra were apodized with a Gaussian multiplication function and Fourier-transformed with one zero-fill. Interpretation of the mass spectra was performed using the *DataAnalysis* v.4.0 software package (Bruker Daltonics, Billerica, Massachusetts, USA).

### 2.9. QM/MM calculations

The 1.2 Å resolution structure reported here (containing only FMN) was prepared by removal of crystal waters and addition of H atoms in the *Maestro* program (Schrödinger). The positions of H atoms were optimized by a short steepest-descent minimization using *Impact* (Schrödinger). In a second system, the crystal geometry of the FMN of chain *A* was replaced by a planarized structure of FMN prepared by geometry optimization *in vacuo* in *Gaussian* 03 (Frisch *et al.*, 2004) using the B3LYP functional with the 6-31G* basis set. This system was used as an alternative starting point for QM/MM optimizations to test convergence with the system starting from the twisted crystal conformation. Redox forms of FMN (oxidized flavin mononucleotide, FMN; anionic semiquinone, $FMN^{-\bullet}$; neutral semiquinone, $FMNH^{\bullet}_{N1}$; anionic hydroquinones, $FMNH^{-}_{N1}$ and $FMNH^{-}_{N5}$, with the proton on N1 or N5, respectively; hydroquinone, $FMNH_2$) positioned in chain *A* of WrbA were selected as the QM region and the protein as the MM region for QM/MM geometry optimization carried out using the program *Qsite* (Schrödinger; Murphy *et al.*, 2000). The DFT method with the B3LYP functional and the 6-31G* basis set was selected as the QM method and the OPLS2005 force field (Jorgensen & Tirado-Rives, 2005) was selected as the MM method. The heavy atoms of the protein were fixed and additional positional restraints were applied to the P and C2′ atoms of the FMN side chain in order to anchor FMN within the protein.

## 3. Results and discussion

### 3.1. WrbA redox activity with FMN and FAD

Fig. 1(*a*) shows the effect of the two cofactors on WrbA redox activity monitored as the rate of oxidation of NADH detected at 340 nm as a function of cofactor concentration. In these early assays, in which substrate concentrations were not optimized, both cofactors yielded the expected sigmoid-shaped response on a semi-log plot, but the two curves were offset by approximately one log unit in flavin concentration, with approximately ten times more FAD than FMN required to reach equivalent activity. TLC analysis of the FAD stocks used for these assays showed only traces of FMN that appeared to be too small to support the measured activity. Activity assays of WrbA with FAD conducted independently on many occasions over several years by various coworkers with different FAD stocks and a range of cofactor incubation times consistently showed an approximately tenfold lower activity compared to WrbA with FMN (data not shown). These early results suggested that FAD may support WrbA redox activity and motivated the crystallization of WrbA with FAD described in the present report, resulting in crystals that contained only FMN as described below.

More recent detailed kinetic analysis of WrbA–FMN (Kishko *et al.*, 2012) defined the optimal conditions and concentrations of components required for measuring WrbA redox activity in various conditions, and indicated that the concentrations of NADH and quinone substrates in the early assays were not suited for quantitative comparison. Fig. 1(*b*) shows the rate of NADH oxidation by WrbA reconstituted with FMN or FAD, or in the absence of protein and cofactor, under conditions where quantitative comparison is meaningful, and with substrate concentrations aimed to minimize potential differences in substrate affinity for active sites

presenting different cofactors. In these conditions the rate of oxidation by WrbA with FMN is approximately three times faster than the rate of oxidation by WrbA with FAD, and the amount of FAD required to attain this rate is 100 times greater than the amount of FMN. Thus, contamination of FAD with as little as 0.3% FMN would be sufficient to account for the apparent catalysis by FAD. Quantitative analysis of the FAD stocks used in these assays by HPLC, with calibration of flavin concentrations, revealed that ∼2–5% FMN is present. The fact that approximately ten times more FMN is present than is indicated by the activity may be accounted for by competition with FAD, which presumably binds to the cavernous WrbA active site even if it does not support redox activity. Binding of FAD is apparently weak, however, as it was not detected (data not shown) under the conditions used previously to determine the affinity of FMN (Grandori *et al.*, 1998).

These results indicate that it is most likely traces of FMN, and not FAD itself, that account for the apparent activity of WrbA with FAD. Nevertheless, the slow-growing crystals formed in the presence of FAD that were already in hand, although containing only FMN as revealed from analysis of their diffraction, proved to diffract to the highest resolution yet reported for this protein; their analysis as detailed here reveals several new features of WrbA.

### 3.2. Structure solution

The slow-growing crystals of WrbA formed in the presence of FAD are here called WrbA–(FAD) to distinguish them from WrbA–FMN crystals grown in the presence of FMN; the parenthetical suffix –(FAD) symbolizes the fact that the slow-growing crystals were found to contain only FMN and not FAD. The structure of WrbA–(FAD) was solved by molecular replacement using the coordinates of *E. coli* WrbA in complex with FMN (PDB entry 2r97; Wolfova *et al.*, 2009) as a search model. The Matthews coefficient of 1.85 Å$^3$ Da$^{-1}$ (Matthews, 1968) and the solvent content of 34% indicate the presence of

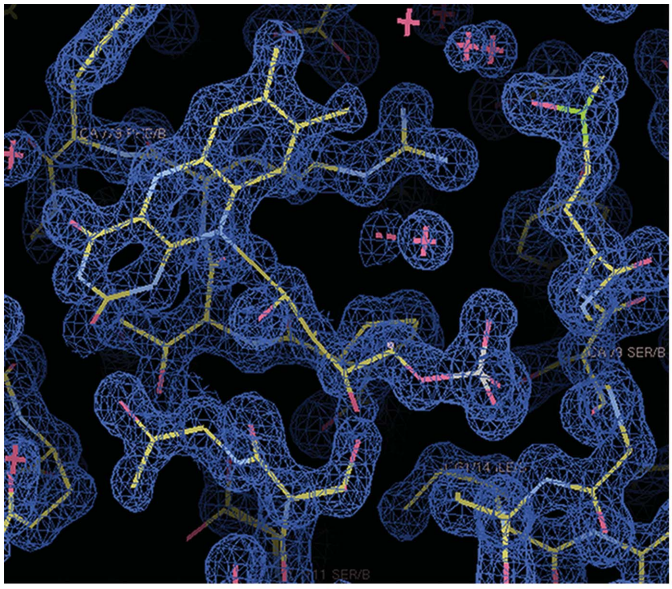

(*a*)

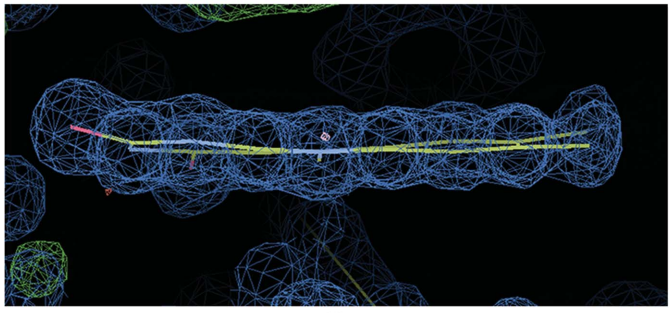

(*b*)

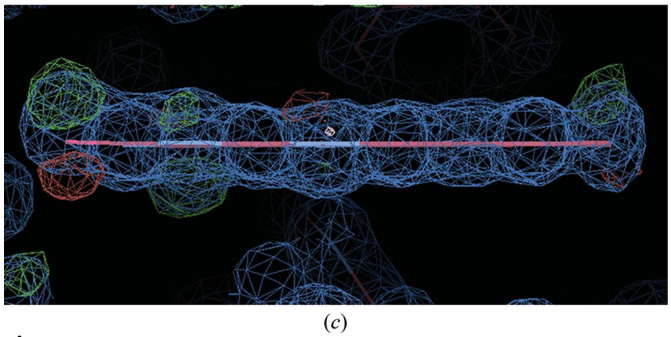

(*c*)

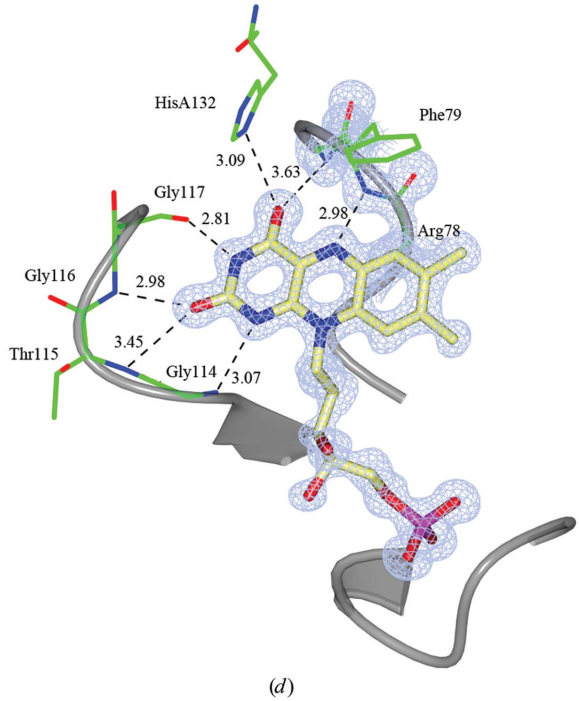


(*d*)

**Figure 2**
FMN. (*a*) Cofactor and its surroundings. Model (lines) and electron density (blue mesh) in the $2F_o - F_c$ map contoured at 1.5$\sigma$. (*b*) Isoalloxazine ring conformation. The view is from the N5 edge of the isoalloxazine ring. Model (lines) and electron density (blue mesh) in the $2F_o - F_c$ map contoured at 1.5$\sigma$. Ring planarity was not restrained during refinement. (*c*) Propeller twist. View as in (*b*). The deviation from planarity for ring atoms was set to 0 Å in the library file during refinement. Positive difference density in the $F_o - F_c$ map (contoured at 3.0$\sigma$) is shown as green mesh and negative difference density as red mesh. (*d*) Hydrogen-bonding network. $2F_o - F_c$ map (blue mesh) around FMN contoured at 1.5$\sigma$ and surrounding protein backbone (grey). Dashed lines and distances indicate potential hydrogen bonds between suitable donor and acceptor groups [atomic colours and yellow (FMN) or green (protein) C atoms] of the protein and cofactor. HisA132 belongs to the second molecule in the asymmetric unit.

two monomers in the asymmetric unit of WrbA–(FAD). The crystal packing is identical to that in a previously described crystal form of WrbA–FMN (PDB entry 2r97; Wolfova *et al.*, 2009), which crystallized in the same space group with an identical solvent content and nearly identical unit-cell parameters, although the crystallization conditions were different. Data-collection and refinement statistics are given in Table 1.

Signs of radiation damage were visible in the structure, as judged by negative peaks in the difference Fourier maps clearly located at the carboxylates of glutamates and aspartates, particularly on solvent-exposed residues Glu23 and Glu146 of molecule *A*. The occupancy of these side-chain atoms was set to 0.7. In molecule *B*, electron density for the side chains of Glu48, Gln172 and Glu176 was weak and these side chains were omitted from the model; in molecule *A*, the side chains of Asp29, Gln145 and Gln152 were similarly not modelled. Carboxylates are prone to radiation-induced decarboxylation (Burmeister, 2000). The distinct susceptibility to radiation damage in each monomer may be explained partly by solvent accessibility in the atomic environment although, as noted by Burmeister, this correlation is imperfect. Several glutamine residues (chain *A* residues 119 and 175 and chain *B* residue 45) showed strong negative density around the side-chain amide group in the difference Fourier map. The occupancies of the affected atoms were set to 0.8. The density for the backbone of loop 167–171 of chain *B* was ambiguous in the simulated-annealing OMIT $F_o - F_c$ map; therefore, this region was also omitted from the model.

### 3.3. Overall structure

The structure of WrbA–(FAD) reported here has the highest resolution amongst available WrbA structures (1.20 Å). The structure consists of two compact monomers in the asymmetric unit with one FMN per monomer, 0.42 Å r.m.s.d. between chains *A* and *B* over 177 aligned residues, and ∼800 Å$^2$ of interface area between monomers. Chain *A* contains 194 residues with residues 154–156 not resolved; chain *B* contains 179 residues with residues 143–155 and 167–171 not resolved. The two monomers of the crystallographic dimer interact across their FMN-binding sites, unlike in apo WrbA (PDB entry 2rg1; Wolfova *et al.*, 2009), in which the two monomers of the crystallographic dimer interact across the equator of the tetramer. Pairwise three-dimensional alignment using the *PDBeFold* server (Krissinel & Henrick, 2004) identified the highest structural alignment match, r.m.s.d. = 0.32 Å, with an *E. coli* WrbA–FMN complex (PDB entry 2r97; Wolfova *et al.*, 2009) solved at 2.0 Å resolution. In a structure of holo WrbA with NADH soaked in (PDB entry 3b6j; Andrade *et al.*, 2007), a PEG fragment was modelled in a position above the FMN isoalloxazine ring. In the corresponding region of the present structure a poorly resolved density in the $F_o - F_c$ map is also present that is discontinuous with all protein and FMN density. This density was not modelled; it cannot accommodate the AMP portion of FAD (data not shown).

The very high resolution sheds new light on a subtle structural feature of WrbA. Secondary-structure assignment (data not shown) using several algorithms [*DSSP* (Kabsch & Sander, 1983), *STRIDE* (Frishman & Argos, 1995), *PROMOTIF* (Hutchinson & Thornton, 1996) and *HELANAL* (Kumar & Bansal, 1996)] shows that previous WrbA structures contain an interruption in helix α3 that might reflect their relatively low resolutions. In the present model helix α3 is in fact split into two helices, α3 and α3′, with an angle of ∼28° between them centred on residue Gln92. Kinked helices, especially those kinked at non-proline sites, are unusual in proteins, and often appear to be relevant for function (Barlow & Thornton, 1988). Consistent with this trend, the pronounced kink in α3 may be functionally significant for WrbA, as the distal half of α3 contains Trp97, which participates directly not only in the active site, but also in both the dimer interface and the tetramer interface (Wolfova *et al.*, 2009).

### 3.4. FMN

Although FAD was used in crystallization, the structure of WrbA–(FAD) reported here contains only FMN. The electron density for FMN is clearly defined, with all non-H atoms accounted for and no contiguous or non-contiguous electron density that could represent the missing adenosine monophosphate portion of FAD (Fig. 2*a*). Thin-layer chromatography (TLC; data not shown) was used to assess the cofactor content of the stock solutions, control solutions, and crystallization droplets. TLC indicates that FMN accumulates to less than ∼5% over months in the FAD stock solutions used, which is consistent with the stability of FAD reported here and previously (Chappelle & Picciolo, 1971). In solutions containing only pure apo WrbA in phosphate buffer/EDTA no detectable conversion of FAD to FMN occurs on the timescale of crystallization, whereas in the WrbA crystallization droplets FAD was converted completely to FMN on this timescale; neither FAD nor AMP could be detected in these samples by TLC. The origin of the presumed FAD-hydrolysing activity in the droplets is unknown at present. Independent repetition of the crystallization and diffraction analysis over a period of ∼1.5 years also only yielded FMN bound in slow-growing crystals (data not shown), but after the subsequent replacement of all solutions crystallization with FAD yielded only apo WrbA crystals (data not shown).

The near-atomic resolution diffraction of the WrbA–(FAD) crystals may reflect the slightly altered crystallization conditions or the concentration-limited incorporation of FMN leading to slower, more ordered crystal growth. To evaluate these possibilities, WrbA crystals were prepared with FMN using the same crystallization conditions as for WrbA–(FAD). Rod-shaped crystals with a deep yellow colour indicative of bound oxidized FMN grew to full size in ∼4 d, unlike the yellow tetragonal bipyramidal crystals of WrbA–(FAD) that required weeks to reach full size. TLC analysis of washed rod-shaped crystals confirms the presence of FMN (data not shown). Three single rod-shaped crystals with large dimensions (0.04 × 0.04 × 0.15–0.2 mm) were chosen as candidates

for diffraction analysis using the same synchrotron-radiation source as for WrbA–(FAD). Analysis of the images by *iMosflm* (Battye *et al.*, 2011) showed that after 30 s exposure the diffraction limit reached only 1.59 Å for the best crystal and 1.7 and 2.0 Å for the other two. These resolution values are similar to those reported by several research groups for tetragonal bipyramidal crystals of WrbA–FMN grown under various crystallization conditions. These findings suggest that the slow incorporation of FMN into WrbA crystals grown with FAD that contains traces of FMN and/or undergoes breakdown of FAD to FMN during crystallization may restrict crystal growth, limiting crystal defects and leading to the very high diffraction resolution discovered here. This hypothesis suggests in turn that high-resolution protein cocrystals might be grown by adding a ligand to an apoprotein in limiting amounts, or gradually in small increments.

### 3.5. Isoalloxazine conformation and redox state

The high resolution of the present data allowed accurate analysis of the FMN isoalloxazine ring conformation, which depends in part on its redox state. The isoalloxazine ring system modelled in the present WrbA–(FAD) structure is not bent but displays a distinct, though relatively small, propeller twist along the length of the ring (Fig. 2*b*). The twisted model fits the $2F_o - F_c$ map and shows no error judging by the difference $F_o - F_c$ map, indicating that it represents the electron density very accurately. Replacing the twisted ring system with a fixed planar isoalloxazine model resulted in both positive and negative peaks in the difference $F_o - F_c$ map (Fig. 2*c*), indicating that a planar ring system accounts less well for the electron density. The functional significance of propeller-twisted FMN in WrbA is unclear. The present structure appears to be the first experimental observation of propeller twisting in a flavoprotein isoalloxazine ring system, although it has been predicted theoretically (Røhr *et al.*, 2010). Propeller twisting does not appear to have been discussed for any of the other very high resolution ($\leq$1.2 Å) protein structures retrieved from the Protein Data Bank using flavin as a keyword and searching the associated publications (data not shown). Just as propeller twisting was observed in DNA single-crystal structures but not fibre-diffraction structures (Dickerson, 1983), it may be detected more often in flavoproteins as additional very high-resolution structures become available.

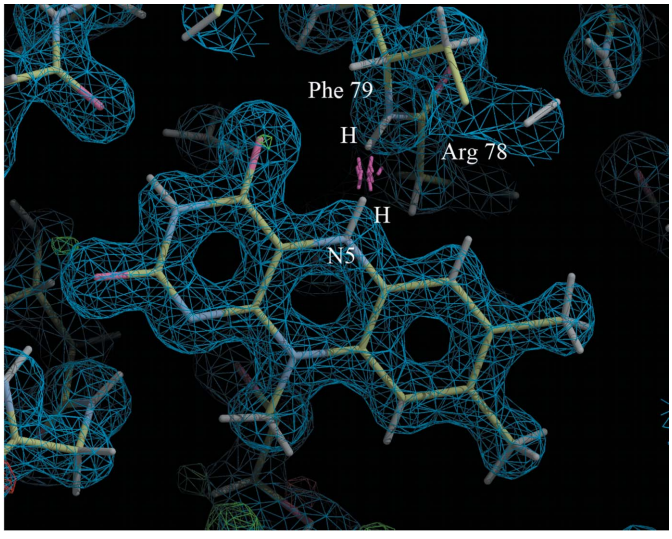


**Figure 3**
Refinement with explicit H atoms. $2F_o - F_c$ map (blue mesh) contoured at 1.2$\sigma$ and positive difference density (green mesh) in the $F_o - F_c$ map contoured at 3.5$\sigma$ after refinement as described in §2 superimposed on stick models of the local structure. The figure is a scene prepared in *Coot* and rendered with *Raster3D*. The clash ('bad overlap contact dots' in *Coot*) between the amide proton of Phe79 and the N5 proton of FMN is represented in pink.

In an effort to assign a specific redox state to the twisted flavin cofactor in the WrbA–(FAD) structure, the protein conformation was evaluated in the vicinity of the isoalloxazine ring. Crystal structures of several flavodoxins in various redox states [as judged in some cases only by the colour of the crystals: *Desulfovibrio desulfuricans* flavodoxin (Romero *et al.*, 1996; PDB entries 3kap for oxidized and 3kaq for reduced), oxidized *Bacillus cereus* flavoprotein NrdI (Røhr *et al.*, 2010; PDB entry 2x2o), *D. vulgaris* flavodoxin (Watt *et al.*, 1991; PDB entries 2fx2, 3fx2 and 4fx2 for oxidized, semi-reduced and reduced, respectively) and *Anacystis nidulans* flavodoxin (Drennan *et al.*, 1999; Hoover *et al.*, 1999, PDB entries 1czn, 1czl and 1d04 for oxidized, semi-reduced and reduced, respectively)] suggest a correlation with protein backbone conformation to accommodate protonation at isoalloxazine position N5 upon reduction. In all structures of oxidized flavodoxins a backbone amide group faces N5 and the adjacent carbonyl group of the preceding residue points away from N5. In other redox states the carbonyl group instead faces N5, except for one structure of a reduced flavodoxin (*A. nidulans*; PDB entry 1d04) in which the amide points toward N5. This analysis indicates that conformation alone cannot rule out reduced flavin, but it suggests that a conformation in which an amide group faces N5, as is found for the Arg78-Phe79 peptide bond in the present structure of WrbA–(FAD), is most strongly correlated with oxidized flavin.

To further evaluate the flavin redox state in these crystals, refinement of atomic coordinates was carried out including explicit H atoms as described in §2 to examine distances near isoalloxazine position N5. The results of this refinement test show that an amide proton on Phe79 and a proton on N5 of FMN cannot be accommodated in the available space without a steric clash (Fig. 3). The distance between the two N atoms is 1.56 Å, and another 0.59 Å would be required to avoid a clash. The results thus exclude the possibility that the WrbA–(FAD) crystals contain FMN redox states with protonated N5 (the anionic hydroquinone $FMNH^-_{N5}$ or the hydroquinone $FMNH_2$). The oxidized state of the flavin would be most consistent with the deep yellow colour of these crystals and the fact that the protein was entirely handled in air, as well as with the failure to detect any stable semiquinone forms of the flavin during the reduction cycle of WrbA–FMN (Nöll *et al.*, 2006).

In recent years it has become apparent that flavin conformation is not a definitive feature for assigning flavoprotein redox state, because flavin conformation is found to be quite variable in all redox states and is differentially influenced by protein environment (Berkholz *et al.*, 2008; Senda *et al.*, 2009; Røhr *et al.*, 2010). Early theoretical studies using *ab initio* molecular orbital calculations in vacuum or water (Zheng & Ornstein, 1996) predicted approximately planar structures for oxidized FMN and for the one-electron-reduced neutral and anionic semiquinones ($FMNH^{\bullet}$ and $FMN^{-\bullet}$); different degrees of so-called butterfly bending between the pyrimidine and benzene rings along the axis defined by atoms N5 and N10, due to electron repulsion that destabilizes the planar conformation were predicted for the two-electron-reduced neutral and anionic hydroquinones ($FMNH_2$, $FMNH^{-}_{N1}$ and $FMNH^{-}_{N5}$). More recently, Røhr *et al.* (2010) demonstrated the potential effect of the protein environment on cofactor conformation by quantum-mechanical/molecular-mechanical (QM/MM) simulations in frozen protein environments using 1.12 and 1.15 Å resolution structures of the *B. cereus* flavoprotein NrdI. A slight propeller twist was predicted for oxidized FMN and for the neutral semiquinone ($FMNH^{\bullet}$) in this specific protein environment. Although the twisted isoalloxazine conformation was not observed in those protein crystals, the results suggest that high-resolution electron densities can be used to assign redox states by comparison with the results of QM/MM simulations.

With the aim of evaluating the FMN redox state in the protein environment of the 1.2 Å resolution WrbA–(FAD) structure, QM/MM simulations were carried out, and the degree of matching between the QM/MM results and the high-resolution electron-density maps available for this structure was evaluated by using superposition r.m.s.d.s. As described in §2, six forms of FMN (FMN, $FMN^{-\bullet}$, $FMNH^{\bullet}_{N1}$, $FMNH^{-}_{N1}$, $FMNH^{-}_{N5}$ and $FMNH_2$) were used in turn as the QM part, and the frozen protein environment was used as the MM part, with additional constraints to ensure the maintenance of the bound state of FMN. The respective r.m.s.d.s relative to the crystal structure for these six forms are 0.232, 0.239, 0.268, 0.304, 0.525 and 0.609 Å. The four species yielding the highest r.m.s.d. values ($FMNH^{\bullet}_{N1}$, $FMNH^{-}_{N1}$, $FMNH^{-}_{N5}$ and $FMNH_2$) display a pronounced bend between the benzene and pyrimidine rings in the QM/MM results that clearly contradicts the electron density. The FMN and $FMN^{-\bullet}$ forms display comparably small r.m.s.d. values and a slight, and very similar, propeller twist in the QM/MM results like that observed in the WrbA–(FAD) crystal. The results thus cannot distinguish between the oxidized and anionic semiquinone redox states.

The finding that even oxidized FMN, which was previously thought to be planar (Zheng & Ornstein, 1996), is predicted to adopt a twisted conformation in the protein environment suggests a strong influence of the protein. In WrbA–(FAD) the backbone amide groups of Gly residues at positions 80, 114, 116, and 117, the backbone amides of Thr115 and Phe79 and the side chain of His132 of the neighbouring subunit are in sufficient proximity to permit hydrogen bonding with FMN isoalloxazine (Fig. 2*d*). Such an extensive network could enforce the twisted conformation of the isoalloxazine ring system.

FMN can be reduced by photoelectrons generated by X-rays during data collection (Berkholz *et al.*, 2008; Røhr *et al.*, 2010), obscuring the functional significance of observed redox states and conformations. Røhr *et al.* (2010) have advocated the use of Raman microscopy before and after irradiation to assess flavoprotein crystals for reduction by photoelectrons. Such experiments are planned for WrbA crystals similar to Raman crystallography recently applied to spinach PsbP (Kopecky *et al.*, 2012).

### 3.6. Methionine oxidation

In previous structures of WrbA (PDB entries 3b6i, 1.66 Å resolution, and 2r97, 2.0 Å resolution) the terminal methyl group of Met10 was modelled in two alternative conformations. Modelling of Met10 as a methionine sulfoxide in the present structure (Fig. 4*a*) agrees very well with a positive peak in the Fourier difference map and would permit hydrogen bonding to the active-site Arg78 side chain as well as to neighbouring water molecules. Refinement of Met10 with two methyl positions does not adequately account for the observed electron density (Fig. 4*b*). Furthermore, the *B*-factor values along the Met10 side chain are all similar, consistent with low mobility of the terminal methyl group. The present findings strongly suggest that previous lower resolution structures probably also represented a single conformation of Met10 sulfoxide rather than two conformations of Met10.

Mass spectrometry establishes that singly oxygenated, doubly oxygenated and non-oxygenated forms of the WrbA polypeptide chain are present in protein samples used for crystallization (native WrbA, $[M+H]^+$ 20 702.42 Da, theoretical mass 20 702.39 Da; singly oxygenated WrbA, $[M+H]^+$ 20 718.35 Da, theoretical mass 20 718.38 Da; doubly oxygenated WrbA, $[M+H]^+$ 20 734.34 Da, theoretical mass 20 734.38 Da). The most intense charge states of the singly oxygenated parent ions, 18+, were fragmented by collision-induced dissociation and the resulting N-terminal b ions were used to evaluate the sites of oxygenation (data not shown). Ions b5, b6, b7 and b8 were not oxygenated, whereas ion b15 was singly oxygenated, consistent with a singly oxygenated site localized on the Met10 side chain. MS data do not identify a unique second site in the doubly oxygenated state (not shown), nor could refinement of the structure model (not shown) assign any other Met residue unambiguously in an oxidized state to account for the second oxygenation detected by MS.

In the present structure, allowed rotations of side-chain dihedral angles could bring the S atom of a non-oxidized Met10 as close as ∼3.1 Å to the closest predicted H atom of the isoalloxazine C8 methyl group without encountering any steric clashes (data not shown). In fact, such a position of the Met10 side chain is very similar to the observed position of Met10 (3.8 Å from the C8 methyl C atom to the Met10 S atom; Fig. 4*c*) in the 1.85 Å resolution crystal structure of apo WrbA (PDB entry 2rg1; Wolfova *et al.*, 2009) after superposition with

the present WrbA–(FAD) model, suggesting that Met10 is positioned for oxidation upon binding of FMN. Thus, oxidation of Met10 may be FMN-dependent, following an electron-transfer path involving the methylbenzene ring. Such a reaction may have occurred during purification of native WrbA, which is carried out in air with the native FMN cofactor copurifying through the first step (Grandori *et al.*, 1998), and presumably leaves the isoalloxazine ring in a partially reduced state. However, in the second purification step the weakly bound FMN is lost and the protein is purified as the apoprotein. Reconstitution prior to crystallization or assaying uses fresh oxidized cofactor, erasing any evidence of the potential involvement of FMN in the oxidation of Met10. Nevertheless, these findings suggest a defined but presently unknown functional role for Met10 oxidation. It may act as a general antioxidant, as has been found in other systems (Luo & Levine, 2009), but further experiments are needed to explore whether Met10 sulfoxide plays any role in the function or stability of WrbA. A similar case is found in the haem lignin peroxidase from the white-rot fungus *Phanerochaete chrysosporium*, in which a surface tryptophan is stereospecifically hydroxylated at $C^{\beta}$ during the redox cycle (Choinowski *et al.*, 1999; Blodig *et al.*, 2001).

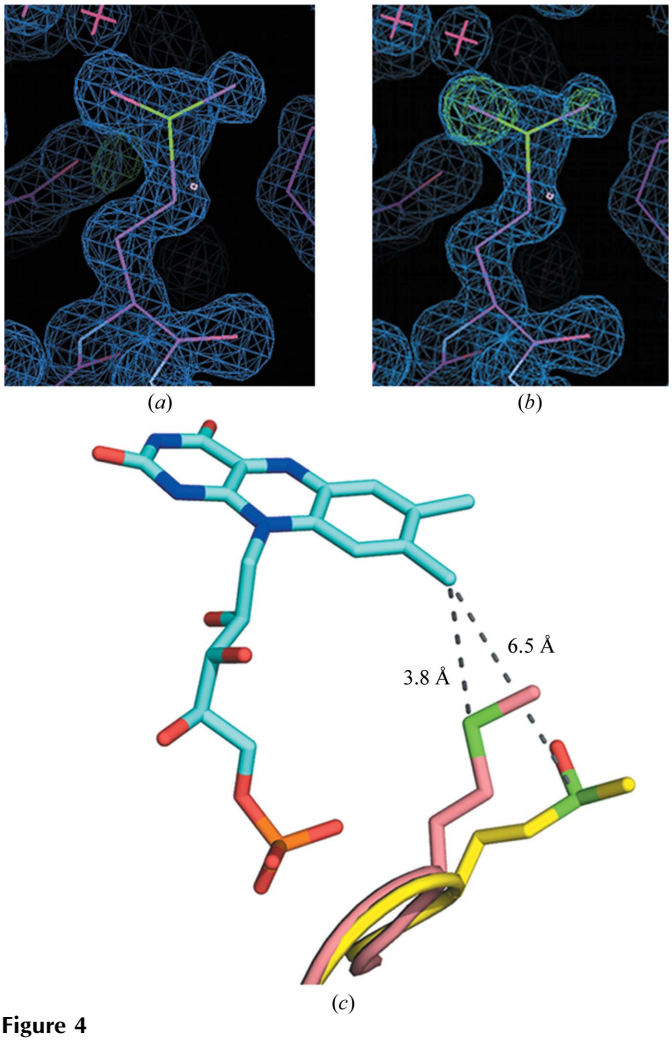


**Figure 4**
Methionine oxidation. (*a*) Met10 sulfoxide. Model (lines) and electron density (blue mesh) in the $2F_o - F_c$ map contoured at $1.5\sigma$. (*b*) Non-oxidized Met10. Model (lines) with occupancies of 0.5 in two alternative conformations and positive difference density (green mesh) of the $F_o - F_c$ map contoured at $3\sigma$. (*c*) Distance to FMN. Met10, Met10 sulfoxide, and FMN (atomic colours and cyan C atoms) are shown as cartoon models after superposition of the 1.85 Å resolution apo WrbA structure (PDB entry 2rg1; pink C atoms) onto the present high-resolution structure of WrbA–(FAD) (yellow C atoms). Dashed lines connect the C atom of the isoalloxazine C8 methyl group to each S atom (green), with the distances indicated.

## 4. Conclusions

The present crystallization of WrbA–(FAD) was motivated by early assays that suggested that FAD supports WrbA redox activity. Subsequent results indicated that traces of FMN contaminating the FAD stocks were likely to be responsible for the apparent activity with FAD. Crystals of WrbA–(FAD) yielded the highest resolution diffraction yet reported for this protein, but analysis of those data showed that only FMN was bound. The resulting 1.2 Å resolution structure reveals new features. The most significant of these is that the FMN isoalloxazine ring system adopts a propeller-twisted conformation that has been predicted but apparently not observed previously in experiments. The redox state of the cofactor is most probably oxidized. Met10 within contact distance of FMN isoalloxazine is oxidized to the sulfoxide. Trp97 resides at the confluence of active site, dimer interface, and tetramer interface, accommodated by a 28° kink at Gln92 in helix $\alpha$3.

The authors express thanks to Catherine A. Lawson for discussion, and to the Helmholtz Zentrum Berlin for access to the BL14.2 beamline. This work was supported by the Czech Science Foundation (P207/10/1934), joint Czech–US International Research Cooperation (ME09016), US NSF OISE-0853423, US NSF DBI-1004830 and Charles University (project UNCE_204025/2012).

## References

Adams, P. D. *et al.* (2010). *Acta Cryst.* D**66**, 213–221.
Andrade, S. L., Patridge, E. V., Ferry, J. G. & Einsle, O. (2007). *J. Bacteriol.* **189**, 9101–9107.
Barlow, D. J. & Thornton, J. M. (1988). *J. Mol. Biol.* **201**, 601–619.
Battye, T. G. G., Kontogiannis, L., Johnson, O., Powell, H. R. & Leslie, A. G. W. (2011). *Acta Cryst.* D**67**, 271–281.
Burmeister, W. P. (2000). *Acta Cryst.* D**56**, 328–341.
Berkholz, D. S., Faber, H. R., Savvides, S. N. & Karplus, P. A. (2008). *J. Mol. Biol.* **382**, 371–384.
Blodig, W., Smith, A. T., Doyle, W. A. & Piontek, K. (2001). *J. Mol. Biol.* **305**, 851–861.
Carey, J., Brynda, J., Wolfová, J., Grandori, R., Gustavsson, T., Ettrich, R. & Smatanová, I. K. (2007). *Protein Sci.* **16**, 2301–2305.
Chappelle, E. W. & Picciolo, G. L. (1971). *Methods Enzymol.* **18**, 381–385.
Chen, V. B., Arendall, W. B., Headd, J. J., Keedy, D. A., Immormino, R. M., Kapral, G. J., Murray, L. W., Richardson, J. S. & Richardson, D. C. (2010). *Acta Cryst.* D**66**, 12–21.
Choinowski, T., Blodig, W., Winterhalter, K. H. & Piontek, K. (1999). *J. Mol. Biol.* **286**, 809–827.
Dickerson, R. E. (1983). *J. Mol. Biol.* **166**, 419–441.
Drennan, C. L., Pattridge, K. A., Weber, C. H., Metzger, A. L., Hoover, D. M. & Ludwig, M. L. (1999). *J. Mol. Biol.* **294**, 711–724.

Ducruix, A. & Giegé, R. (1999). *Crystallization of Nucleic Acids and Proteins. A Practical Approach*, 2nd ed. Oxford University Press.
Emsley, P. & Cowtan, K. (2004). *Acta Cryst.* D**60**, 2126–2132.
Evans, P. (2006). *Acta Cryst.* D**62**, 72–82.
Frisch, M. J. *et al.* (2004). *Gaussian* 03, Revision C.02. Gaussian Inc., Wallingford, Connecticut, USA.
Frishman, D. & Argos, P. (1995). *Proteins*, **23**, 566–579.
Gorman, J. & Shapiro, L. (2005). *Protein Sci.* **14**, 3004–3012.
Grandori, R. & Carey, J. (1994). *Protein Sci.* **3**, 2185–2193.
Grandori, R., Khalifah, P., Boice, J. A., Fairman, R., Giovanielli, K. & Carey, J. (1998). *J. Biol. Chem.* **273**, 20960–20966.
Hoover, D. M., Drennan, C. L., Metzger, A. L., Osborne, C., Weber, C. H., Pattridge, K. A. & Ludwig, M. L. (1999). *J. Mol. Biol.* **294**, 725–743.
Hutchinson, E. G. & Thornton, J. M. (1996). *Protein Sci.* **5**, 212–220.
Jorgensen, W. L. & Tirado-Rives, J. (2005). *Proc. Natl Acad. Sci. USA*, **102**, 6665–6670.
Kabsch, W. & Sander, C. (1983). *Biopolymers*, **22**, 2577–2637.
Kishko, I., Harish, B., Zayats, V., Reha, D., Tenner, B., Beri, D., Gustavsson, T., Ettrich, R. & Carey, J. (2012). *PLoS One*, **7**, e43902.
Kopecky, V., Kohoutova, J., Lapkouski, M., Hofbauerova, K., Sovova, Z., Ettrichova, O., González-Pérez, S., Dulebo, A., Kaftan, D., Smatanova, I. K., Revuelta, J. L., Arellano, J. B., Carey, J. & Ettrich, R. (2012). *PLoS One*, **7**, e46694.
Krissinel, E. & Henrick, K. (2004). *Acta Cryst.* D**60**, 2256–2268.
Krissinel, E. & Henrick, K. (2007). *J. Mol. Biol.* **372**, 774–797.
Kumar, S. & Bansal, M. (1996). *Biophys. J.* **71**, 1574–1586.
Leslie, A. G. W. (2006). *Acta Cryst.* D**62**, 48–57.
Li, R., Bianchet, M. A., Talalay, P. & Amzel, L. M. (1995). *Proc. Natl Acad. Sci. USA*, **92**, 8846–8850.
Luo, S. & Levine, R. L. (2009). *FASEB J.* **23**, 464–472.
Matthews, B. W. (1968). *J. Mol. Biol.* **33**, 491–497.
Mayhew, S. G. & Tollin, G. (1991). *Chemistry and Biochemistry of Flavoenzymes*, edited by F. Müller, Vol. 3, pp. 389–426. Boca Raton: CRC Press.
McNicholas, S., Potterton, E., Wilson, K. S. & Noble, M. E. M. (2011). *Acta Cryst.* D**67**, 386–394.
Merritt, E. A. & Bacon, D. J. (1997). *Methods Enzymol.* **277**, 505–524.
Mueller, U., Darowski, N., Fuchs, M. R., Förster, R., Hellmig, M., Paithankar, K. S., Pühringer, S., Steffien, M., Zocher, G. & Weiss, M. S. (2012). *J. Synchrotron Rad.* **19**, 442–449.
Murphy, R. B., Philipp, D. M. & Friesner, R. A. (2000). *J. Comput. Chem.* **21**, 1442–1457.
Murshudov, G. N., Skubák, P., Lebedev, A. A., Pannu, N. S., Steiner, R. A., Nicholls, R. A., Winn, M. D., Long, F. & Vagin, A. A. (2011). *Acta Cryst.* D**67**, 355–367.
Nöll, G., Kozma, E., Grandori, R., Carey, J., Schödl, T., Hauska, G. & Daub, J. (2006). *Langmuir*, **22**, 2378–2383.
Patridge, E. V. & Ferry, J. G. (2006). *J. Bacteriol.* **188**, 3498–3506.
Røhr, A. K., Hersleth, H. P. & Andersson, K. K. (2010). *Angew. Chem. Int. Ed. Engl.* **49**, 2324–2327.
Romero, A., Caldeira, J., Legall, J., Moura, I., Moura, J. J. & Romao, M. J. (1996). *Eur. J. Biochem.* **239**, 190–196.
Senda, T., Senda, M., Kimura, S. & Ishida, T. (2009). *Antioxid. Redox Signal.* **11**, 1741–1766.
Vagin, A. & Teplyakov, A. (2010). *Acta Cryst.* D**66**, 22–25.
Watt, W., Tulinsky, A., Swenson, R. P. & Watenpaugh, K. D. (1991). *J. Mol. Biol.* **218**, 195–208.
Wolfova, J., Smatanova, I. K., Brynda, J., Mesters, J. R., Lapkouski, M., Kuty, M., Natalello, A., Chatterjee, N., Chern, S. Y., Ebbel, E., Ricci, A., Grandori, R., Ettrich, R. & Carey, J. (2009). *Biochim. Biophys. Acta*, **1794**, 1288–1298.
Yang, W., Ni, L. & Somerville, R. L. (1993). *Proc. Natl Acad. Sci. USA*, **90**, 5796–5800.
Zheng, Y. & Ornstein, R. L. (1996). *J. Am. Chem. Soc.* **118**, 9402–9408.